Electrowetting on Semiconductors

Cesar Palma[1, a)] and Robert Deegan[1, b)]
University of Michigan

(Dated: 11 December 2014)

Applying a voltage difference between a conductor and a sessile droplet sitting on a thin dielectric film separating it from the conductor will cause the drop to spread. When the conductor is a good metal, the change of the drop's contact angle due to the voltage is given the Young-Lippmann equation. Here we report experiments with lightly-doped, single crystal silicon as the conductive electrode. We derive a modified Young-Lippmann equation that includes effects due to the semiconductor and contact line pinning. We show that light induces a non-reversible wetting transition, and that our model agrees well with our experimental results.

Electrowetting is a phenomenon wherein the wetting properties of liquid on a solid substrate are modified by the application of a voltage[1]. The effect has been exploited for microfluidic actuation[2], adjustable lenses[3] and electronic displays[4]. In the basic electrowetting-on-dielectric (EWOD) experimental configuration a sessile drop of electrolyte rests on a thin insulator separating it from an electrode, typically a good conductor. Applying a voltage between the drop and the electrode induces spreading and a concomitant reduction of the drop's contact angle θ. This phenomenon is well modeled up until the onset of contact angle saturation[1] by the Young-Lippmann equation:

$$\cos\theta = \cos\theta_o + \frac{1}{2}\frac{cV^2}{\gamma_{\mathrm{lv}}} \tag{1}$$

but only if the electric field is almost entirely confined to the insulator, as is the case for a metal electrode. Here V is the applied bias, c is the capacitance per unit area of the insulator and θ_o is the zero-bias equilibrium contact angle given by Young's equation: $\cos\theta_o = (\gamma_{\mathrm{sv}} - \gamma_{\mathrm{sl}})/\gamma_{\mathrm{lv}}$, where γ_{xy} refers to the respective interfacial tensions between the liquid (l), solid (s), and vapor (v).

Arscott[5] observed novel electrowetting effects when the conductor is replaced by a semiconductor. He showed that, unlike the case of a metal electrode, the response of the contact angle was asymmetric with respect to the polarity of the applied bias and that light induced a reversible wetting transition, a phenomenon he termed *photoelectrowetting*. He distinguished three electrowetting regimes and associated these with the charge distributions known from metal-insulator-semiconductor devices: accumulation, inversion, and deep depletion. Arscott modeled his results using the Young-Lippmann equation with c replaced by the small-signal capacitance (dQ/dV). More recently he revisited these experiments[6] and proposed a new model where $\frac{1}{2}cV^2$ is replaced by the electrostatic energy density of the charge distributions.

Chiou et al.[7] studied electrowetting on hydrogenated amorphous silicon under AC biasing. These authors too find a light-induced wetting transition they term *opto-electrowetting*[8] and demonstrated the capacity to linearly translate pico-liter sized droplets. They explained their results using the photo-conductive property of the silicon films, and model the contact angle response using the Young-Lippmann equation with the DC bias replaced by the RMS voltage across the dielectric.

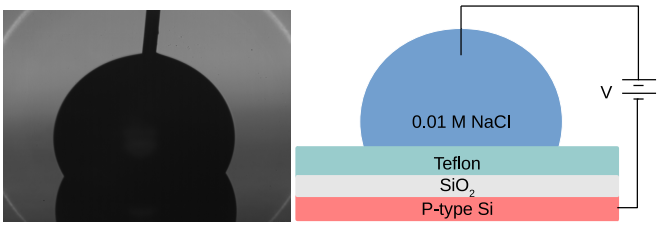

FIG. 1. Experimental configuration. Left: image from infrared camera for contact angle measurement. Right: Schematic of device configuration (not to scale).

Here we present the results of our electrowetting experiments on single crystal silicon. We derive from thermodynamics a modified version of the Young-Lippmann equation to account for the penetration of the electric field into the semiconductor. We show that it is essential to consider non-idealized effects such contact line pinning, interface traps, and work function differences. Our measurements agree well with this model. Contrary to the results of Arscott[5] we show that photoelectrowetting is non-reversible by light alone because it is a transition from a non-equilibrium to an equilibrium state.

As argued by Arscott[5], the drop-liquid-insulator-semiconductor stack closely resembles the metal-insulator-semiconductor (MIS) device that is the core of the MOS field effect transistor. When a bias is applied to the metal gate in an MIS device, the corresponding charge distribution can exhibit three distinct equilibrium states depending on the magnitude and polarity of the applied bias relative to the doping type of the crystal: accumulation, depletion and inversion. It is also possible to induce deep depletion, a non-equilibrium charge distribution, formed by rapidly ramping the bias towards inversion. Due to the slow generation rate of minority carriers, the charge distribution remains in the depleted state but with a much deeper depletion width than it

[a)] czarv@umich.edu
[b)] rddeegan@umich.edu

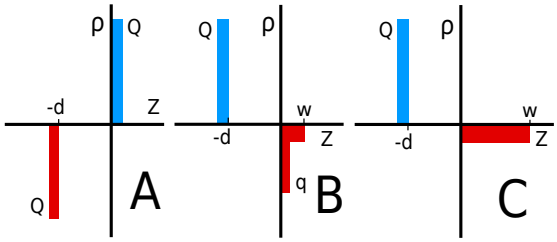

FIG. 2. Charge distributions for p-type MIS device under: (a) accumulation, (b) inversion and (c) deep depletion. The metal lies on the interval $z < -d$, the insulator $-d < z < 0$, and the semiconductor $z > 0$.

would otherwise attain in equilibrium[9]. The charge distribution for these states are depicted in fig. 2.

To compute the equilibrium contact angle for electrowetting, we minimize the free energy F with respect to area, holding the temperature, volume, and charge constant. The free energy has contributions from surface tension and the electrostatic fields. The former is $\gamma_{\rm sl}A - \gamma_{\rm sv}A + \gamma_{\rm lv}S$ where A is the contact area of the drop and S the area of the liquid-vapor interface, and the latter is $U = \frac{1}{2}\int d^3x\ \vec{D}\cdot\vec{E}$. Thus,

$$\left(\frac{\partial F}{\partial A}\right)_{V,Q,T} = \gamma_{\rm sl} - \gamma_{\rm sv} + \gamma_{\rm lv}\left(\frac{\partial S}{\partial A}\right)_V + \left(\frac{\partial U}{\partial A}\right)_Q = 0 \quad (2)$$

It can be shown[10] that $\left(\frac{\partial S}{\partial A}\right)_V = \cos\theta$, from which it follows that

$$\cos\theta = \cos\theta_o - \frac{1}{\gamma_{\rm lv}}\left(\frac{\partial U}{\partial A}\right)_Q \quad (3)$$

We calculate $\left(\frac{\partial U}{\partial a}\right)_Q$ from a generic charge distribution $\rho(x)$ that includes the charge distributions of fig. 2 as special cases:

$$\rho(z) = \frac{Q}{A}\delta(z+d) - \frac{q}{A}\delta(z) - eN(H(z) - H(z-w)) \quad (4)$$

where Q is the total charge imposed by an external potential, N is the density of ionized acceptors, e is the elementary charge, w is the width of the depletion region, δ is the delta function, and H is the Heaviside function. Charge neutrality requires $w = (Q-q)/(eNA)$. Equation 4 uses the depletion approximation[9] in which the charge density in the depletion zone drops to zero as a step function. For now, we also neglect nonideal MIS effects such as work function differences and oxide charges.

We compute the electric field E from eq. 4, and from this $U = \frac{A}{2}\int_{-d}^{w} dz\ \epsilon E^2$, $\left(\frac{\partial U}{\partial A}\right)_Q$ and the voltage drop $V = \int_{-d}^{w} dz\ E$:

$$\left(\frac{\partial U}{\partial A}\right)_Q = -\frac{\Sigma^2}{2c} - \frac{(\Sigma-\sigma)^3}{3\lambda} - \frac{(\Sigma-\sigma)^2}{2\lambda}\left(\frac{\partial q}{\partial A}\right)_Q \quad (5)$$

$$V = \frac{\Sigma}{c} + \frac{(\Sigma-\sigma)^2}{2\lambda} \quad (6)$$

where c is the net capacitance of the dielectric per unit area ($c = \frac{\epsilon_i}{d}$ for a single dielectric layer with permittivity ϵ_i), $\Sigma = Q/A$, $\sigma = q/A$, $\lambda = \epsilon_s eN$ and ϵ_s is the permittivity of the silicon crystal.

In accumulation $q = Q$ and eqs. 3, 5 and 6 reduce to:

$$\cos\theta = \cos\theta_o + \frac{c}{2\gamma_{\rm lv}}V^2 \quad (7)$$

Following a rapid ramp, the semiconductor will be in deep depletion and $q = 0$. In deep depletion then,

$$\cos\theta = \cos\theta_o + \frac{\lambda^2}{3\gamma_{\rm lv}c^3}\left[-1 - 3\tilde{V} + (1+2\tilde{V})^{3/2}\right] \quad (8)$$

where $\tilde{V} = c^2V/\lambda$. We note that eq. 8 was reported by Arscott and Gaudet[6] though their method of derivation is different than our own.

While in deep depletion $q = 0$, but as the electrons thermalize q will rise until the semiconductor is inverted. A small depletion layer will remain in inversion, but our numerical calculations indicate that more than 99% of the electrostatic energy is confined within the insulators and so $q \approx Q$ and eq. 7 is an excellent approximation for the contact angle response in inversion.

The deep depletion state forms because the generation rate of minority carriers is slow in very pure semiconductors such as prime silicon wafers. But shining light of wavelength shorter than the corresponding bandgap energy on a semiconductor rapidly generates minority carriers[11] and thus greatly accelerates the approach to equilibrium. During an electrowetting experiment the system brought into deep depletion by a step-like change in the bias and then illuminated almost instantly changes to inversion. Thus, the net change in contact angle due to illumination is given by the difference of eqs. 7 & 8. Note however that the role of light is to drive the system towards equilibrium, and thus the process is not reversible, i.e. turning off the light will not restore the original deep depletion state.

We tested our predictions (eqs. 7 & 8) on electrowetting devices formed on p-type silicon 4" (100) wafers doped with Boron. Wafer resistivity was measured with four-point probe to be $\rho = 15.7$ Ω-cm from which the doping concentration N was inferred to be $8.6 \times 10^{14}\text{cm}^{-3}$. The wafer was prepared by the following sequence of steps. A 100 nm layer of silicon dioxide was grown by dry oxidation (1 hr, 25 mins at 1000 °C with followed by N_2 annealing at the same temperature for 10 minutes). Trans-LC, a chlorine containing compound, was added during oxidation to neutralize mobile ionic charge. Ohmic contacts were fabricated by removing the oxide from target areas by mechanical abrasion with a diamond scribe, depositing a layer of aluminum by physical vapor deposition through a patterned metal mask, and annealing for five minutes at 500 °C in an Argon atmosphere. Two contacts were fabricated on each device and current-voltage measurements indicated that these were good ohmic contacts. A second insulator film made

of teflon was deposited on the oxide by spin coating a 2% (w/w) solution of Teflon AF 1600 solids (DuPont) dissolved in FC-40 (Sigma-Aldrich) for 20 seconds at 500 rpm and 30 seconds at 1000 rpm followed by annealing steps for 15 minutes at 183 °C and 15 minutes at 330°C in a 1 atm N_2 atmosphere. The oxide and teflon layer thicknesses were measured by ellipsometry to be $d_s = 101$ nm and $d_t = 265$ nm, respectively. Together with the literature values for the permittivities of silicon dioxide ($3.9\epsilon_o$) and Teflon AF ($1.93\epsilon_o$), yields an expected value for c of 5.4×10^{-5} F/m^2.

We evaporated gold contacts on to the Teflon surface to measure the device's capacitance-voltage characteristics. Figure 3 compares a device with a single film of Teflon to one with a bilayer of Teflon and thermally grown oxide. The former exhibited much stronger hysteresis and thus we exclusively used the latter in our experiments.

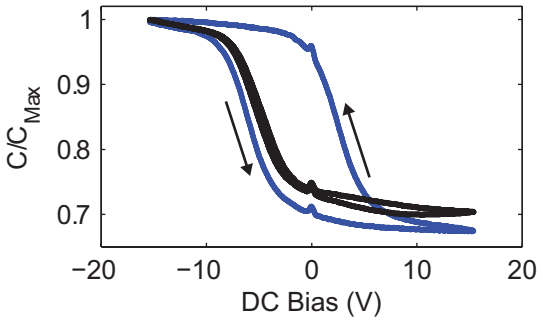

FIG. 3. Capacitance versus voltage for a Au-Teflon-Si (blue, 0.2 V/s, 1 KHz) and a Au-Teflon-SiO_2-Si (black, 0.1 V/s, 1 KHz) capacitor.

Our experiments were done with a 10 mM NaCl aqueous solution. Its surface tension was measured to be 72 mN/m. A 5 μl drop was pipetted on to the teflon layer and a 0.14 mm steel wire was inserted into the apex of the drop (see Fig. 1). Voltages were applied across the wire and ohmic contacts with a source-measurement unit (Keithley 2400 SMU) and the contact angle was extracted by processing a digital image of the drop. Current monitoring allowed observation of possible dielectric breakdown. To prevent photo-generation of minority carriers the experiments were performed in complete darkness. The drop was backlit with an infrared LED (λ = 1550 nm) and imaged with an infrared-sensitive camera (FLIR A2600sc). A typical image is shown in Fig. 1. To study the response of the drop to light a high power white LED (MCWHL5, Thorlabs) was used for illumination.

Our measurements in accumulation and inversion were made by increasing the voltage in one volt steps starting at 15 volts because below this voltage we saw no change in the contact angle. In deep depletion the measurements were taken at 5 volt steps to limit minority carrier generation during the experiment. At each step, following a short period (300 ms) for electrostatic and hydrodynamic equilibration, an image was recorded. To

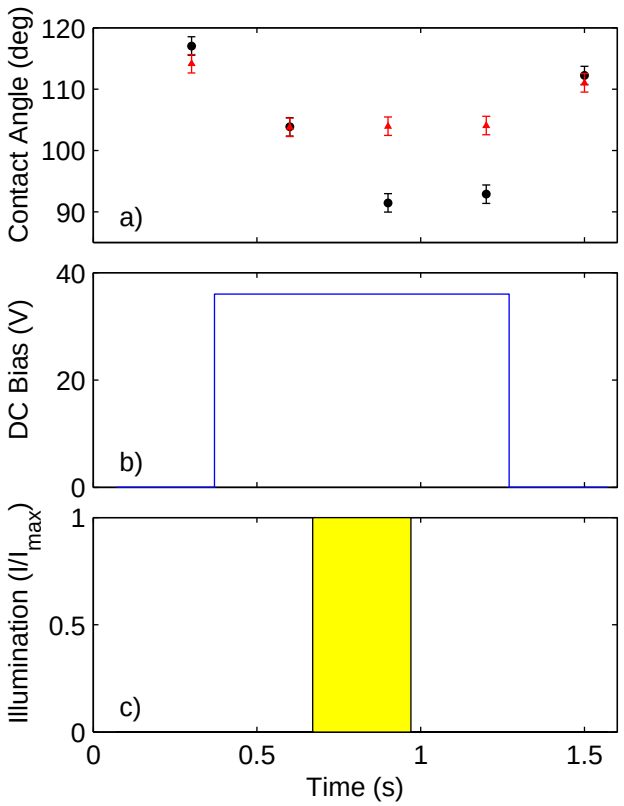

FIG. 4. a) Contact angle versus time in an electrowetting experiment where the drop is illuminated (black circles) and not illuminated (red triangles). b) Applied bias vs time for both experiments. c) Illumination vs time for illuminated experiment normalized to full intensity (19 mW/cm^2). Note that turning off the illumination does not restore the pre-illumination value and that in the absence of illumination the second wetting transition does not occur. Error bars indicate reproducibility from run to run.

produce the inversion data sets, the LED was mounted in close proximity, aimed at the droplet and activated at full intensity (19 mW/cm^2) for 200 ms following application of the voltage. A typical measurement of the photo-electrowetting effect is shown in fig. 4 (black circles). These data show a decrease in the contact angle following the application of a bias, followed by another decrease upon illuminating the drop. As expected from our analysis, turning off the light source does not restore the contact angle to it's pre-illumination value.

A summary of all our experiments is given in fig. 5. Between ±15 V there were no observable changes of the contact angle, indicating contact line pinning[10]. To account for this pinning threshold, we modified our model by replacing the equilibrium contact angle with the advancing contact angle θ_a based on the following rationale. When the drop is first deposited on the surface, it spreads until the contact angle falls below the advancing contact angle. As the bias is increased the stress on the contact line increases until it exceeds the pinning thresh-

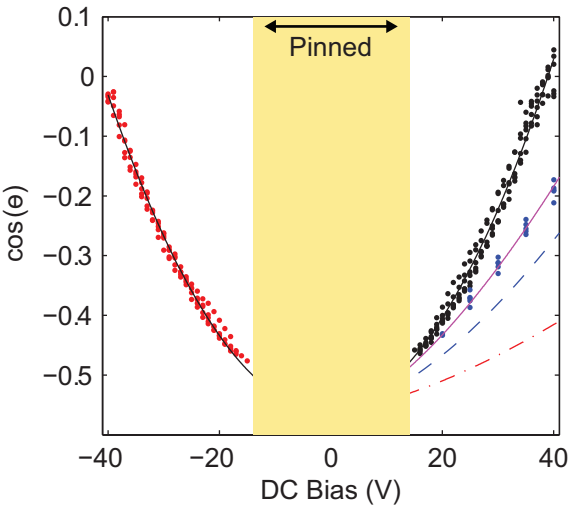

FIG. 5. Electrowetting on moderately doped p-type semiconductor for accumulation (red circles), deep depletion (blue circles), and inversion (black circles) – color available online. The solid black line is a fit to the Young-Lippmann equation with a voltage offset. The dashed blue line is a plot of eq. 8 with the parameters obtained from fitting the accumulation and inversion data, and the solid magenta line is the same model with the addition of interface traps (eqn. 9). Red dot-dashed line depicts the earlier deep depletion model proposed by Arscott[5]. No change in contact angle is observed beneath a certain magnitude for the applied bias, shown as pinned region.

old. Thus the advancing contact angle gives a measure of the pinning threshold, and its inclusion in our model accounts for this additional force on the contact line. Additionally, an asymmetry around zero volts in the form of an offset is apparent in the data. MIS capacitors are known to exhibit a shift in the flatband voltage[11] as a result of fixed oxide charges and work function differences between the silicon and the metal. Thus, we introduce a horizontal offset by replacing V with $(V - V_o)$ in our model to account for these effects.

We compared our model to the data. We first fit the accumulation and inversion data sets to eq. 7 and extracted the fittting parameters c, $\cos\theta_a$ and the bias offset V_o. The fit yields $c = 5.0 \times 10^{-5}$ F/m^2, which is 7% lower than the value expected from thickness measurements, and a flatband offset of -1.1 V. Using these fit parameters and the measured values of the doping concentration and electrolyte surface tension the deep depletion prediction was computed from eq. 8. The result is plotted in fig. 5 as a dashed blue line; the model predicts a larger contact angle than observed.

We considered various effects that might account for the discrepancy between our model and measurements, and rejected all but one of these. We considered whether stray fields at the edges of the drop and the finite Debye length in the silicon were responsible. A finite element calculations for the free energy in depletion that took these into account agree with eq. 8 to within 0.5%. We considered whether minority carrier generation through R-G center thermal recombination, or stray light leaking into our enclosure was prematurely inverting the charge distribution. We also consider whether the inertia of fluid was causing the contact line to overshoot the equilibrium value. In any of these cases, the discrepancy ought to exhibit a ramp rate dependence. However, ramp rates at 1 V/s and 5 V/s showed identical results.

Finally, we considered interface traps. Localized electronic states with energies in the forbidden gap are well known to appear at the Si/SiO_2 interface[9]. These states are found throughout the bandgap and are in electrical contact with the bulk. Unlike minorities carriers, interface states with energies close to the valence band respond quickly to changes in the surface potential. We note however that a transition from one interface trap to another is an unlikely event even when these two are close in energy given realisitic values for trap densities at the Si/SiO_2 interface and their highly localized nature. Figure 6 depicts the interface traps and their proposed occupancy at $V = V_{offset}$, in depletion, deep depletion and inversion. In eq. 4, where we previously assumed $q = 0$ in deep depletion, we substitute $q = \sigma A$ where σ is the areal density of occupied traps. Combining eqns. 3, 5 & 6 and $(\partial q/\partial A)_Q = \sigma$ yields the prediction for deep depletion corrected for surface states:

$$\cos\theta = \cos\theta_a + \frac{\lambda^2}{3\gamma_{lv}c^3}\left[-1 + 3\tilde{\sigma} - \frac{3}{2}\tilde{\sigma}^2 + 3(\tilde{\sigma}-1)\tilde{V} + (1 + 2\tilde{V} - 2\tilde{\sigma})^{3/2}\right] \quad (9)$$

where now $\tilde{V} = c^2(V - V_o)/\lambda$ and $\tilde{\sigma} = c\sigma/\lambda$. A fit of the data to eq. 9 with σ as a free parameter and using the previously obtained values of c, $\cos\theta_a$ and V_o gives a value of $\sigma = 1.8 \times 10^{-11}$cm^{-2} that is well within the bounds for our fabrication process[12]. Thus, we believe that the discrepancy is due to interface traps.

In summary, we measured the photoelectrowetting effect on single crystal silicon. We find that there is an irreversible spreading actuated by light when the device is biased towards inversion. We introduced an idealized model for this effect and derive expressions for the contact angle as function of voltage. Our measurements show a discrepancy between the data and the ideal model. With the introduction of non-ideal effects due to contact line pinning, flat-band offset, and interface traps, our model accurately captures the phenomena of photo-

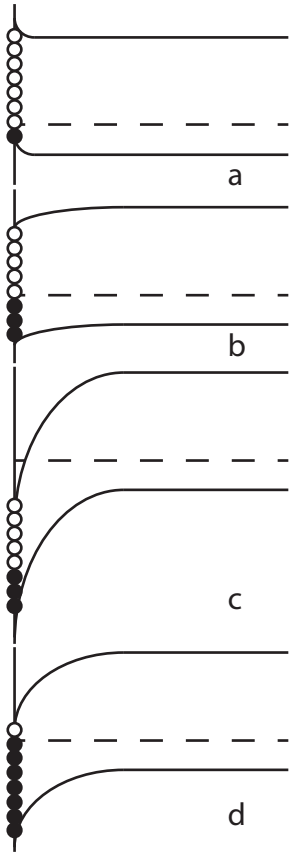

FIG. 6. Band diagrams showing: (a) Trap occupancy at $V = V_{offset}$, (b) in depletion, (c) deep depletion and (d) inversion. Filled circles depict occupied states while empty circles depict unoccupied states. The dashed line represents the Fermi energy level. Note that only the states close to the valence band with short time constants change occupancy. The time constant increases exponentially with distance from the valence band and so deeper interface states are essentially inaccessible during fast sweeps. Thus in changing the voltage from depletion to deep depletion, the number of filled interface states remains unaltered. In inversion all states below the Fermi level are occupied as this is an equilibrium state.

electrowetting.

ACKNOWLEDGMENTS

We are grateful for the assistance of Pilar Herrera-Fierro, Nadine Wang, Tom Latowski, Matthew Oonk and Brian Armstrong at the Lurie Nanofabrication Facility and for support from DARPA under Young Faculty Award.

[1] F. Mugele and J.-C. Baret, Journal of Physics: Condensed Matter **17**, R705 (2005).
[2] M. G. Pollack, R. B. Fair, and A. D. Shenderov, Applied Physics Letters **77**, 1725 (2000).
[3] B. Berge and J. Peseux, The European Physical Journal E **3**, 159 (2000).
[4] R. A. Hayes and B. Feenstra, Nature **425**, 383 (2003).
[5] S. Arscott, Scientific reports **1** (2011).
[6] S. Arscott and M. Gaudet, Applied Physics Letters **103**, 074104 (2013).
[7] P. Chiou, S.-Y. Park, and M. C. Wu, Applied Physics Letters **93**, 221110 (2008).
[8] P. Y. Chiou, H. Moon, H. Toshiyoshi, C.-J. Kim, and M. C. Wu, Sensors and actuators A: physical **104**, 222 (2003).
[9] E. H. Nicollian, J. R. Brews, and E. H. Nicollian, MOS (metal oxide semiconductor) physics and technology, vol. 1987 (Wiley New York et al., 1982).
[10] P.-G. De Gennes, F. Brochard-Wyart, and D. Quéré, Capillarity and wetting phenomena: drops, bubbles, pearls, waves (Springer, 2004).
[11] S. M. Sze and K. K. Ng, Physics of semiconductor devices (John Wiley & Sons, 2006).
[12] W. Beadle, J. Tsai, and R. Plummer, Quick reference manual for silicon integrated circuit technology (Wiley New York, 1985).